^{87}Sr, ^{119}Sn, ^{127}I Single and {^{1}H/^{19}F}-Double Resonance Solid-State NMR Experiments: Application to Inorganic Materials and Nanobuilding Blocks

Danielle Laurencin,[b] François Ribot,[a] Christel Gervais,[a] Adrian J. Wright,[c] Annabelle R. Baker,[d] Lionel Campayo,[e] John V. Hanna,[f] Dinu Iuga,[f] Mark E. Smith,[f,g] Jean-Marie Nedelec,[h] Guillaume Renaudin,[h] and Christian Bonhomme[a]*

Abstract: ^{87}Sr, ^{127}I and ^{119}Sn wideline NMR spectroscopy was successfully applied to inorganic and hybrid materials: *(i)* Sr derivatives of medicinal interest (Sr-malonate, Sr-pyrophosphates, mixed Ca,Sr-fluoroapatites) ; *(ii)* apatitic structures acting as host matrices for iodine; and *(iii)* Sn-derived oxo-clusters which can be used as inorganic nanobuilding blocks. The BRAIN (BRoadband Adiabatic INversion) CP (Cross Polarization) approach (by Schurko *et al*.) was applied for the first time to a non integer quadrupolar nucleus (^{87}Sr, I = 9/2). The sequence was used in combination with WURST (Wideband Uniform-Rate Smooth-Truncation) QCPMG (Quadrupolar Carr-Purcell Meiboom-Gill) for optimal sensitivity. We showed that ^{127}I WURST QCPMG experiments were sufficiently sensitive to allow rapid characterization of the incorporation of iodide (I^-) anions in lead vanadate/phosphate apatites, and that ^{127}I acted as a sensitive probe for the description of local disorder. ^{1}H/^{19}F →^{119}Sn BRAIN CP was successfully applied to the detailed characterization of tin oxo-clusters, using ^{1}H and ^{19}F as spin baths. We demonstrated that BRAIN CP can be effectively used as a tool of *spectral editing* leading to the estimation of spatial proximities between ^{119}Sn and ^{1}H/^{19}F nuclei.

[a] Dr F. Ribot, Pr C. Gervais, Pr C. Bonhomme*, Sorbonne Universités, UPMC Univ Paris 06, CNRS, Collège de France, UMR 7574, Chimie de la Matière Condensée de Paris, 75005, Paris, France.
E-mail : christian.bonhomme@upmc.fr
[b] Dr D. Laurencin, Institut Charles Gerhardt de Montpellier, UMR 5253, CNRS-UM-ENSCM, Université de Montpellier, Montpellier, France.
[c] Dr A. J. Wright, School of Chemistry, University of Birmingham, Edgbaston, Birmingham, B15 2TT, UK.
[d] Dr A. R. Baker, Diamond Light Source, Harwell Science and Innovation Campus, Didcot, OX11 0DE, UK.
[e] Dr L. Campayo, CEA, DEN, DTCD, SECM, Laboratoire d'Etude et de Développement de Matrices de Conditionnement, Centre de Marcoule, 30207 Bagnols sur Cèze, France.
[f] Dr J. V. Hanna, Dr D. Iuga, Pr M. E. Smith, Department of Physics, University of Warwick, Coventry, CV4 7AL, UK.
[g] Pr M. E. Smith, Vice-Chancellor's Office, University House, Lancaster University, Lancaster, LA1 4YW, UK.
[h] Dr G. Renaudin, Pr J.-M. Nedelec, ICCF, CNRS UMR 6295, SIGMA Clermont, Université Clermont Auvergne, Campus des Céseaux, CS 20265, Aubière, France.

Introduction

Solid-state NMR is one of the most pertinent tools for investigation of inorganic and hybrid materials from both structural and dynamical points of view.[1] In combination with first principles calculations of magnetic parameters (chemical shift and quadrupolar interactions, indirect J coupling),[2,3] NMR acts as a key ingredient in "NMR crystallography"[4] (a newly introduced concept) and complements nicely X-ray and neutron diffraction techniques. During the last few years, spectacular progress has been made in the design of solid-state NMR pulse sequences devoted to nuclei subjected to strong interaction anisotropies (*wideline* and *ultra-wideline* NMR).[5] For diamagnetic samples, these anisotropies are mainly related to the quadrupolar effect due to the quadrupole moment of a given nucleus (I > 1/2) and/or CSA. Second-order quadrupolar effects are inversely proportional to the static magnetic field, B_0, but can still be dominant even working at the highest field leading to strongly broadened lineshapes.[6,7] In contrast CSA is proportional to B_0 and represents a major source of line broadening at ultra-high magnetic field (in particular for "heavy metals" such as ^{111,113}Cd, ^{117,119}Sn, ^{195}Pt and ^{199}Hg).[6] The price to pay for such broadening of the NMR lines is a drastic *decrease in sensitivity* leading usually to very long acquisition times.

^{87}Sr (I = 9/2) and ^{127}I (I = 5/2) act as prototypes for "strong quadrupolar" nuclei and represent potentially interesting probes in materials science. As an example, strontium derivatives (involving anions such as malonate, $C_3H_2O_4^{2-}$, ranelate, $C_{12}H_6N_2O_8S^{4-}$, and phosphate, PO_4^{3-}) have major applications in medicine (strontium

malonate and ranelate have a marked action against osteoporosis)[8] and in the field of biocompatible materials (mixed calcium-strontium phosphate ceramics and strontium doped bioglasses).[9,10,11,12,13] Moreover, strontium boronates have been developed as a new family of coordination polymers.[14,15] However, ^{87}Sr solid-state NMR experiments have seldom been reported in the literature.[9,14,16,17,18]

Iodine occurs even more widely in materials science, notably because of its variety of oxidation states (from –I to +VII), and because it can be found not only as an anion (e.g. I^-, IO_3^-, IO_4^-…) in inorganic materials, but also as part of an organic molecule in materials constructed on the basis of halogen-bonding interactions for example.[19] Among the different classes of materials involving iodine, those developed in view of the immobilization of radioactive iodine-129, one of the longest half-life radionuclides (~ 16×10^6 years), are worth mentioning.[20] In this context, apatite-based ceramics have been shown to be an attractive and realistic option, allowing the incorporation of iodine in the form of iodide I^- (using mixed vanadate/phosphate lead apatites as host matrices)[21] or iodate IO_3^- (using calcium phosphate apatites).[22] However, despite the importance of iodine in materials science, very few ^{127}I NMR experiments have been reported to date.[23]

^{119}Sn (I = 1/2) can exhibit very strong CSA effects especially at ultra-high magnetic field and acts as well as a local probe of interest in inorganic chemistry.[6,24,25,26,27] As an example of important tin compounds, tin oxo-clusters of general formula $\{(RSn)_{12}O_{14}(OH)_6\}^{2+}$ (noted **$(RSn)_{12}$** thereafter) and $\{RSnO(O_2CR')\}_6$ (noted **$(RSn)_6$** thereafter) (see Figures 4 and 7 for a representation of the oxo-cores; R, R' stand here for organic chains) can be considered as versatile nanobuilding blocks for the synthesis of tunable hybrid O/I materials[28,29,30] which can be used as matrices for photochromic dyes[31], exhibit self-healing properties[32] or improved resistance to oxidation.[33] To the best of our knowledge, very few ^{1}H → ^{119}Sn experiments based on the heteronuclear dipolar interaction have been published so far.[34,35]

In connection with the above-cited topics, and going back to dedicated *wideline* NMR methodology, Schurko and others[5,7,36] implemented smart, robust and efficient methods to record strongly broadened lineshapes in the static mode. Here, key points were: *(i)* the multiple refocusing of magnetization during the FID acquisition (Carr-Purcell Meiboom-Gill echo trains, CPMG or QCPMG for quadrupolar nuclei), *(ii)* the implementation of frequency-stepped pulses (Wideband, Uniform Rate, and Smooth Truncation, WURST)[36] – for uniform excitation of broad powder patterns. Such pulse sequences could be combined with manipulation of the satellite transitions (ST) *prior* to the detection of the central transition (CT) (for example, Double-Frequency Sweeps, DFS[37]) leading to optimal sensitivity. When dealing with lineshapes much broader than the excitation bandwidth, the Variable Offset Cumulative Spectrum VOCS[38] approach could be ultimately implemented. In other words, the strategy followed here could be related to the acronym DFS VOCS WURST QCPMG. It followed that numerous "complex" quadrupolar nuclei such as ^{87}Sr,[9,14,16,17,18] ^{127}I,[39] ^{137}Ba[40], ^{209}Bi[41] could be studied at ultra-high magnetic field with relative ease. Initially, the DFS VOCS WURST QCPMG approach was mainly devoted to the direct *single resonance* detection of quadrupolar nuclei (apart from {^{1}H} decoupling during the acquisition time). It appeared as a theoretical and experimental challenge to extend the concepts cited above to *double resonance* experiments (including for example Cross Polarization (CP) from abundant nuclei – ^{1}H or ^{19}F, as a building block of the NMR sequence). In this case, the excited bandwidth in the standard CP process is related to the strength of the spin lock (SL) rf fields. One way to increase this bandwidth is to use the strongest SL fields compatible with probe specifications. However, considering nuclei subjected to strong quadrupolar and/or CSA anisotropies (and subsequent huge broadening of the lineshapes), it seems unrealistic to achieve full excitation and the rather tedious VOCS CP approach remains the only feasible option. Recently, Schurko and co-workers[42] have elegantly circumvented this drawback by implementing frequency sweep during the CP contact introducing the so-called BRAIN (BRoadband Adiabiatic INversion) sequence. During the frequency sweep, a Hartmann-Hahn (H-H) matching condition is fulfilled for each isochromat in the powder pattern leading to much broader bandwidth and a significant increase of the signal to noise ratio. Moreover, two crucial advantages of BRAIN CP can be particularly stressed, namely: *(i)* the low powers used on both irradiation channels, *(ii)* the possible combination of BRAIN CP with WURST CPMG/QCPMG acquisition. In other words, a fully broadband CP sequence can be implemented. During the past years, Schurko's group has successfully applied the BRAIN CP approach mainly to spin-1/2 isotopes such as ^{119}Sn (dibutyltin(IV) oxide), ^{199}Hg (mercury acetate)[42] and ^{195}Pt ($Pt[NH_3]_4Cl_2$,[42] and Magnus' pink salt[43]). In all cases, ^{1}H was used as the source of polarization (or spin bath). Mastrorilli *et al.*[44] implemented as well the ^{1}H → ^{195}Pt CP CPMG combination for the study of phosphanido-bridged diplatinum complexes (without BRAIN). To the best of our knowledge, BRAIN CP was applied so far to a single *integer* quadrupolar nucleus, ^{14}N (I = 1) (to study glycine, active pharmaceutical derivatives or Magnus's pink salt).[43,45] As first-order quadrupolar interaction was involved (^{14}N Pake doublet), only half of the complete doublet was recorded leading to a net decrease of the experimental time (the complete lineshape was obtained by symmetry). We stress here that the

above mentioned experiments were all implemented in the static mode. Very recently, the extension of BRAIN to MAS conditions was described theoretically by Wi *et al.*[46] (without experimental applications).

In this contribution, we extend for the first time the BRAIN CP approach to the study of half-integer nuclei such as ^{87}Sr (I = 9/2). For this nucleus, it was previously demonstrated that protons (from OH^- groups and/or H_2O molecules) had a crucial impact on the ^{87}Sr NMR acquisition.[9] Indeed, in the case of belovite, $Sr_{10}(PO_4)_6(OH)_2$, no ^{87}Sr DFS WURST QCPMG spectrum could be obtained despite optimization of all experimental parameters (including {^{1}H} decoupling and the temperature of the sample during the NMR experiment). At this stage, we emphasize that belovite is a member of the *apatite supergroup*:[47] the most famous prototype of this particular family of minerals being hydroxyapatite, $Ca_{10}(PO_4)_6(OH)_2$. Here, in order to efficiently implement the BRAIN CP WURST QCPMG experiment and to identify the relevant parameters related to it, *labeled* strontium malonate, *$Sr(CH_2(COO)_2)$, and strontium phenyl-boronate, *$Sr(C_6H_5B(OH)_3)_2.H_2O$, were chosen as pertinent reference samples. Labeled samples were used in order to greatly shorten the experimental time and to allow exploring a large number of independent parameters. The set up of the experiment is indeed crucial as lineshape distortions have to be minimized. *Natural abundance* samples were studied as well and the particular role of $T_1(^1H)$ (compared to $T_1(^{87}Sr)$) was stressed. In this situation, the main advantage of BRAIN CP is mostly related to *spectral editing*[48,49] (in contrast to ^{14}N BRAIN CP results presented by Schurko *et al.*[43,45] where a net increase in signal to noise ratio was the main advantage).

In a second part, we present the study of the incorporation of iodide anions in lead vanadate/phosphate apatite derived materials obtained by various synthetic protocols using ^{127}I NMR. The structure of $Pb_{10}(VO_4)_6I_2$ is comparable to vanadinite, $Pb_{10}(VO_4)_6Cl_2$, another member of the apatite supergroup (see above). We demonstrate that ^{127}I WURST QCPMG (without DFS excitation) is a suitable approach to detect small variations in the obtained spectra, which can be related to subtle changes in the structure of the materials, of general formula, $Pb_{(10-x)}(VO_4)_{4.8}(PO_4)_{1.2}I_{(2-2x)}$. The variations of the ^{127}I NMR spectra can tentatively be related to changes in x.

Finally, several tin oxo-clusters, **$(BuSn)_{12}$** and **$(BuSn)_6$**, are successfully studied by $^1H \rightarrow ^{119}Sn$ and/or $^{19}F \rightarrow ^{119}Sn$ CP/BRAIN CP WURST CPMG experiments, mainly for *spectral editing* purposes. The spectral editing capabilities of BRAIN CP were not demonstrated so far in the literature though potentially adding much value to the experiment. In this case, distinct ^{119}Sn CSA have to be taken into account as 5 and 6 fold coordinated Sn atoms are present in the structures. Realistic structural schemes could be obtained, which is particularly interesting given that crystallographic structures have not been determined by X-ray diffraction techniques for these compounds. In that context, **$(BuSn)_{12}(O_3SCF_3)_2$** is an interesting challenge as both ^{1}H and ^{19}F polarizations can be used as the polarization source in BRAIN CP transfers. With this material, ^{19}F nuclei are used as a spin bath for the first time.

The overall objective of this article being to extend and make more accessible to a wide range of chemical practitioners wideline acquisition methods (including the BRAIN-CP sequence) to an extended variety of materials. We emphasize the impact of a large number of instrumental parameters in the Experimental Section and propose a step-by-step implementation of these sequences.

Experimental Section

Materials syntheses

Crystalline α-$Sr_2P_2O_7$, amorphous $Sr_2P_2O_7.4H_2O$ and $Sr(PO_3F)$ were synthesized implementing the following protocols. **α-$Sr_2P_2O_7$**: 1.0 mol.L^{-1} of $SrCl_2$ solution was stirred whilst an equal volume of 0.2 mol.L^{-1} $K_4P_2O_7$ solution was added to it. Following the addition of the $K_4P_2O_7$ solution, the resulting precipitate was immediately recovered *via* vacuum filtration, washed with deionized water and methanol, and left to dry at room temperature (RT) overnight. **Amorphous $Sr_2P_2O_7.4H_2O$**: 1.0 mol.L^{-1} of $Sr(NO_3)_2$ solution was stirred whilst an equal volume of 0.2 mol.L^{-1} $K_4P_2O_7$ solution was added to it. Following the addition of the $K_4P_2O_7$ solution, the resulting precipitate was immediately recovered *via* vacuum filtration, washed with deionized water and methanol, and left to dry at RT overnight. Heat treatment involved the sample to 200°C in an oven for 1 hour in air before cooling to RT. **$Sr(PO_3F)$**: a 2 mol.L^{-1} solution of $SrCl_2$ was added to a stirred 1 mol.L^{-1} solution of $Na_2(PO_3F)$ dropwise in equal volumes with a solution kept at 80°C. The resulting white precipitate was collected via vacuum filtration, washed thoroughly with deionized water and dried at RT in air overnight.

The precipitation method was used to synthesize the fluorapatite sample of nominal composition **$Ca_5Sr_5(PO_4)_6F_2$**. Two solutions of 100 mL containing stoichiometric amount, with respect with apatite composition, of respectively dissolved F^-/PO_4^{3-} and dissolved Ca^{2+}/Sr^{2+} species were prepared with respectively the targeted amount of ammonium fluoride (NH_4F), ammonium dihydrogenphosphate ($(NH_4)H_2PO_4$), Sigma-Aldrich, CAS number 7722-76-1), calcium nitrate tetrahydrate ($Ca(NO_3)_2{\cdot}4H_2O$, Sigma-Aldrich, CAS number 13477-34-4) and strontium nitrate ($Sr(NO_3)_2$, 99.995%, Sigma-Aldrich , CAS number 10042-76-9). The

pH of both solutions has been controlled using 30% volumetric ammonium hydroxide solution in water ("ammonia water", NH_4OH, Sigma-Aldrich, CAS number 1336-21-6), whose starting pH was about 13. F^-/PO_4^{3-} and Ca^{2+}/Sr^{2+} containing solutions were controlled and set respectively to pH = 10 and pH = 11. After equilibrating the pH solutions, the F^-/PO_4^{3-} solution was added drop wise in about 3 hours to the Ca^{2+}/Sr^{2+} containing solution under a nitrogen atmosphere. The formation of a white precipitate was observed already at the beginning of the addition. The pH was monitored and kept over 10 by adding the necessary volume of ammonia water after 90 minutes (half of total mixing time) and at the end of mixing. Then the white solution was left under gentle stirring for 24 hours at room temperature under nitrogen. The obtained precipitate was then filtered through a paper filter supported on a Büchner funnel connected to a low-vacuum pump (~ 200 mbars). The powder was rinsed twice with ethanol (96% pure) and twice with water. The white precipitate was dried on a glass support to 105°C overnight. The powder was finally crushed into a fine powder and heat treated 4 hours at 900°C (10°C.min^{-1}), to obtain a crystalline powder. X-ray powder pattern and Rietveld analyses of the data are given in Figure SI-1a).

The syntheses of *labeled* (^{87}Sr) and non-labeled Sr-malonate phases are described in ref 9. The ^{87}Sr-labeled Sr-phenylboronate phase was synthesized starting from ^{87}Sr-labeled *$SrCO_3$ (CortecNet, 90% labeled in ^{87}Sr). First, 125 mg of enriched *$SrCO_3$ (0.85 mmol, 1 equiv) was placed in an alumina crucible and heated to 1000°C under a stream of Ar to form *SrO (heating rate: 5°C/min; dwell time: 1.5h), and the sample was then left to cool at room temperature under a stream of Ar. Then, 206 mg of phenylboronic acid (1.7 mmol, 2 equiv) were dissolved in 1.2 mL of a 1/1 EtOH/H_2O mixture, and the *SrO solid was added progressively under stirring. The suspension was sonicated and then stirred overnight at room temperature, after which it was centrifuged. The supernatant was removed and the white solid dried twice with diethylether and then further dried under vacuum at room temperature (100 mg, yield: 65%). The FTIR spectra of Sr-phenylboronate (labeled and non-labeled) are presented in Figure SI-1b.

$Pb_{10}(VO_4)_6I_2$ was synthesized according to previously established procedures, by calcination of a stoichiometric mixture of $Pb_3(VO_4)_2$ and PbI_2 for 3 hours at 700 °C in an air-tight sealed container.[50] A $Pb_{(10-x)}(VO_4)_{4.8}(PO_4)_{1.2}I_{(2-2x)}$ phase (referred to as sample **4** below) was prepared under similar conditions, starting from $Pb_3(VO_4)_{1.6}(PO_4)_{0.4}$ and PbI_2.[51] Other $Pb_{(10-x)}(VO_4)_{4.8}(PO_4)_{1.2}I_{(2-2x)}$ phases (samples **1**, **2**, **3** and **5** below) were synthesized starting from the same reagents, but using a different experimental process, namely reactive Spark Plasma Sintering (as described by Le Gallet *et al.*)[21] These samples differed slightly in terms of temperature of synthesis and ratio between reagents, and the ones with the highest value of "x" are those obtained at the highest temperature (**4**) or starting with the largest deficiency in PbI_2 (**3** and **5**). We stress here that it was quite impossible to estimate the small variations of "x" for the series of samples as they were within the uncertainty range of the measurements. For further characterization, powder XRD patterns for $Pb_{10}(VO_4)_6I_2$ and samples **1** to **5** are presented in Figure SI-2.

$\{(BuSn)_{12}O_{14}(OH)_6\}(OH)_2$ (thereafter **$(BuSn)_{12}(OH)_2$**) and $\{(BuSn)_{12}O_{14}(OH)_6\}SO_4$ (thereafter **$(BuSn)_{12}SO_4$**) were synthesized as previously reported.[52,53] $\{(BuSn)_{12}O_{14}(OH)_6\}(O_3SCF_3)_2$ (thereafter **$(BuSn)_{12}(O_3SCF_3)_2$**) was synthesized by reacting 2 eq. of HO_3SCF_3 (triflic acid) with 1 eq. of $\{(BuSn)_{12}O_{14}(OH)_6\}(OH)_2$ dissolved in THF (10 w%). The mixture was stirred for 1 hour and then all the volatiles were removed under vacuum. The resulting crude solid was crystallized in acetonitrile (yield = 73%). The compound was characterized by multinuclear solution NMR spectroscopy in $CDCl_3$. Chemical shifts are given in ppm and scalar couplings in Hz. ^{119}Sn NMR (111.9 MHz): −283.6 (CN=5) and −466.9 (CN=6), with $^2J(^{119}Sn_{CN=5}\text{-}^{119}Sn_{CN=6}) = 425$, $^2J(^{119}Sn_{CN=5}\text{-}^{117}Sn_{CN=5}) = 154$, $^2J(^{119}Sn_{CN=6}\text{-}^{117}Sn_{CN=6}) = 175$. ^{19}F NMR (282.4 MHz): −78.16 (CF_3). ^{1}H NMR (300.13 MHz): 5.60 (s, μ_2-OH), 1.75 (quint., $C\underline{H}_2CH_2Sn_{CN=5}$), 1.63 (t, $C\underline{H}_2Sn_{CN=5}$), 1.63 (quint., $C\underline{H}_2CH_2Sn_{CN=6}$), 1.49 (sext., $C\underline{H}_2CH_2CH_2Sn_{CN=5}$), 1.35 (sext., $C\underline{H}_2CH_2CH_2Sn_{CN=6}$), 1.24 (t, $C\underline{H}_2Sn_{CN=6}$), 0.95 (t, CH_3), 0.88 (t, CH_3). We stress here on the fact that *no crystallographic structure is currently available for* ***$(BuSn)_{12}(O_3SCF_3)_2$***.

$[BuSnO(O_2CC_6H_4NH_2)]_6$ (hereafter **$(BuSn)_6(O_2CC_6H_4NH_2)_6$**) was prepared as previously reported.[54]

Solid-state NMR spectroscopy

All solid-state NMR spectra were recorded using Bruker Avance II/III 850 MHz spectrometers (ν_0 = 850.22, 799.94, 36.85, 170.11, 317.05 MHz for ^{1}H, ^{19}F, ^{87}Sr, ^{127}I and ^{119}Sn, respectively) and single-resonance low gamma 7 mm X, double-resonance 4 mm HX, double-resonance 4 mm HX low-gamma and triple-resonance 4 mm HXY(^{19}F) Bruker probes (used mostly in static mode).

^{87}Sr spectra were obtained by implementing DFS WURST QCPMG and ^{1}H CP/BRAIN CP WURST QCPMG flip back sequences (see NMR schemes in Figure SI-3). The optimized parameters were: DFS: convergence sweep and duration noted {kHz,kHz,μs}; WURST acquisition: number of points used for the shape, sweep width and duration noted {points,kHz,μs} in Table SI1, power level used on the ^{87}Sr channel (here: $|\omega_1(^{87}Sr)|/2\pi$ = 8.6 kHz); QCPMG: number of echoes, spikelet separation; number of scans, relaxation delay. For

^{1}H BRAIN CP WURST QCPMG flip back, the optimized parameters were: ^{1}H relaxation delays by recording ^{1}H synchronized MAS Hahn echoes spectra of the samples, $t_{90°}$–τ–$t_{180°}$–τ–acquisition ($\nu_{rot.}$ = 10 kHz, $t_{90°}(^{1}H)$ = 4.8 μs, refocusing delay, τ: one rotor period); contact time, t_{CP}; power levels on ^{1}H and ^{87}Sr channels ($\omega_1(^{1}H)/2\pi$ = 16.5 and $|\omega_1(^{87}Sr)|/2\pi$ = 2.4 kHz, respectively); the flip back pulse on ^{1}H ($t_{90°}(^{1}H)$ = 4.8 μs) was located just after the CP block for improved efficiency (compared to the situation where the ^{1}H flip back pulse was located after the QCPMG echo train). Continuous wave (CW) {^{1}H} decoupling was applied when necessary. Particular attention was paid to the design of the contact time WURST shape in the ^{1}H BRAIN CP WURST QCPMG flip back experiment: the number of points used for the shape was of particular importance (especially for long contact time, t_{CP} > 30 ms). For the contact pulse, the optimized parameters were: number of points used for the shape, sweep width and duration noted {points,kHz,μs} in Table SI1; power levels on the ^{1}H and ^{87}Sr channels ($\omega_1(^{1}H)/2\pi$ = 21.9 kHz and $|\omega_1(^{87}Sr)|/2\pi$ = 3.8 kHz, respectively).

Experimental observations: *(i)* The ratio $|\omega_1(^{1}H)/\omega^{1}(^{87}Sr)|$ is an important parameter to optimize in order to avoid lineshape distortions under BRAIN conditions. This point was clearly demonstrated by Schurko *et al*.[42] through implementing spin dynamics calculations. Consequently, and apart from BRAIN CP implementation, it seemed important to record a direct DFS WURST QCPMG spectrum for direct comparison of the lineshapes. *(ii)* the absence of residual direct Zeeman direct magnetization was carefully checked at each step. *(iii)* The use of a RAMP[55] pulse on the ^{1}H channel during t_{CP} had no significant effect. *(iv)* when necessary, the VOCS approach was implemented. The number and value of the offsets (in kHz) are given in Table SI1. *(v)* The sensitivity of the BRAIN CP experiment was enhanced by implementing a special type of shape. The idea here was to "add" consecutive BRAIN WURST shapes to obtain a given contact time. As an example, t_{CP} = 100 ms was obtained by the "addition" of two 50 ms WURST shapes.

^{127}I spectra were obtained using two types of sequences: the static solid echo (at a fixed offset), $t_{90°}$–τ–$t_{90°}$–τ–acquisition, with adequate phase-cycling, and VOCS WURST QCPMG. No DFS was applied here as sensitivity was intrinsically high for all experiments. Optimized parameters: WURST: number of points used for the shape, sweep width and duration noted {points,kHz,μs}, power level used on the ^{127}I channel (here: $\omega_1(^{127}I)/2\pi$ = 22.1 kHz); QCPMG: number of echoes, spikelet separation; number of scans, relaxation delay. The number and value of the offsets (in kHz) are given in Table SI2.

^{119}Sn spectra were obtained by implementing WURST CPMG and ^{1}H/^{19}F CP/BRAIN CP WURST CPMG sequences (no flip back of the ^{1}H magnetization as $T_1(^{1}H/^{19}F)$ values were short enough for the studied samples). The optimized parameters were: WURST: number of points used for the shape, sweep width and duration noted {points,kHz,μs}, power level used on the ^{119}Sn channel (here: $|\omega_1(^{119}Sn)|/2\pi$ = 45.5 kHz); CPMG: number of echoes, spikelet separation; number of scans, relaxation delay. CP WURST CPMG: the optimized parameters were: ^{1}H relaxation delays by recording the ^{1}H spectra ($\nu_{rot.}$ = 14 kHz, $t_{90°}(^{1}H)$ = 5.0 μs); contact time, t_{CP}; power levels on ^{1}H and ^{119}Sn channels ($\omega_1(^{1}H)/2\pi$ = 71.4 and $|\omega_1(^{119}Sn)|/2\pi$ = 72.2 kHz, respectively). CW {^{1}H} decoupling was applied when necessary (30.0 kHz only, as acquisition time could be very long). For ^{1}H/^{19}F BRAIN CP WURST CPMG, the optimized parameters were: number of points used for the shape, sweep width and duration noted {points,kHz,μs} in Table SI3; power levels on the ^{1}H, ^{19}F, and ^{119}Sn channels ($\omega_1(^{1}H)/2\pi$ = 27.7, $\omega_1(^{19}F)/2\pi$ = 29.4, and $|\omega_1(^{119}Sn)|/2\pi$ = 41.2 kHz, respectively). ^{19}F MAS spectra were obtained at $\nu_{rot.}$ = 10-14 kHz with $t_{90°}(^{19}F)$ = 2.0 μs (without {^{1}H} high power decoupling).

^{1}H chemical shifts were referenced with respect to TMS (tetramethylsilane) using adamantane as a secondary reference (1.85 ppm). ^{19}F chemical shifts were referenced using a secondary reference, namely **(BuSn)$_{12}$**(O_3SCF_3)$_2$ ($\delta(^{19}F)$ = –78.16 ppm in $CDCl_3$ solution: a value of –78.0 was used as reference for $\delta_{iso}(^{19}F)$ in the solid state). ^{87}Sr NMR spectra were referenced against a 1.0 M aqueous solution of $SrCl_2$ (0.0 ppm, relaxation delay: 0.1 s). A 0.1 M aqueous solution of $SrCl_2$ led to a signal at –0.8 ppm.[9] ^{127}I NMR spectra were referenced using secondary references, namely NaI and KI ($\delta_{iso}(^{127}I)$ = 226.7 and 192.6 ppm, respectively – fast single pulse MAS experiments). Such a secondary calibration of ^{127}I spectra was suggested by Bryce *et al*.[39a] ^{119}Sn spectra were referenced using a secondary reference, namely, **(BuSn)$_{12}$**$(OH)_2$ ($\delta_{iso}(^{119}Sn)$ = –275.0 ppm[25] for the most deshielded resonance, $CSnO_4$).

Solution NMR experiments were carried out on a Bruker Avance III 300 spectrometer, operating at 300.13, 282.4 and 111.92 MHz for ^{1}H, ^{19}F and ^{119}Sn, respectively, equipped with a 5mm Bruker BBFO probe. ^{1}H chemical shifts are referenced with respect to TMS using the protonated impurity of $CDCl_3$ as a secondary internal reference (7.26 ppm). ^{19}F chemical shifts are referenced with respect to $CFCl_3$. ^{119}Sn chemical shifts are referenced towards tetramethyltin (TMT).

First principles calculations of ^{87}Sr and ^{127}I NMR parameters

The NMR chemical shift calculations were performed within the DFT formalism using the QUANTUM-ESPRESSO (QE) software.[56] The

PBE generalized gradient approximation[57] was used and the valence electrons were described by norm conserving pseudopotentials[58] in the Kleinman-Bylander form[59] except for Sr, I and V (PAW method in the implementation of Kresse and Joubert) which were generated by Prof. Dal Corso and exported from the THEOS web site.[60] The wave functions were expanded on a plane wave basis set with a kinetic energy cut-off of 1088 eV. The shielding tensor is computed using the GIPAW[61] approach which permits the reproduction of the results of a fully converged all-electron calculation. The isotropic chemical shift δ_{iso} is defined as $\delta_{iso} = -[\sigma - \sigma^{ref}]$, where σ is the isotropic shielding and σ^{ref} is the isotropic shielding of the same nucleus in a reference system. In the present case, the comparison between the calculated and experimental data is presented in Table SI4 for *(i)* SrO, $SrCO_3$, $Sr(NO_3)_2$ SrF_2 and $SrCl_2$ and *(ii)* CaI_2, MgI_2 and CdI_2 for ^{87}Sr and ^{127}I, respectively. The slopes of the linear correlations were fitted freely and allowed extraction of σ^{ref} for both nuclei.

Diagonalization of the symmetrical part of the calculated tensor then provides its principal components σ_{11}, σ_{22}, σ_{33} from which the chemical shift components δ_{11}, δ_{22}, δ_{33} can be calculated. δ_{11}, δ_{22} and δ_{33} are defined such as $|\delta_{33} - \delta_{iso.}| \geq |\delta_{11} - \delta_{iso.}| \geq |\delta_{22} - \delta_{iso.}|$, and $\delta_{iso.} = 1/3(\delta_{11} + \delta_{22} + \delta_{33})$. The CSA parameters are defined by $\delta_{CSA} = \delta_{33} - \delta_{iso.}$ and $\eta_{CSA} = |(\delta_{22} - \delta_{11})/ \delta_{CSA}|$. The principal components V_{xx}, V_{yy}, and V_{zz} of the electric field gradient (EFG) tensor defined as $|V_{zz}| \geq |V_{xx}| \geq |V_{yy}|$ are obtained by diagonalization of the tensor. The quadrupolar interaction can then be characterized by the quadrupolar coupling constant C_Q and the asymmetry parameter η_Q, which are defined as: $C_Q = eQV_{zz}/h$ and $\eta_Q = (V_{yy} - V_{xx})/V_{zz}$ (e is the proton charge, h Planck's constant and Q the quadrupole moment of the considered nucleus). The experimental value of the quadrupole moment of ^{87}Sr ($Q = 30.5 \times 10^{-30}$ m^2) and ^{127}I ($Q = -69.6 \times 10^{-30}$ m^2)[62] were was used to calculate C_Q. All simulations of the NMR spectra were performed by using the DMFit software available on the web (free of charge) (Qstat1/2 and int2QUAD modules were used for quadrupolar only and combined quadrupolar/CSA interactions, respectively).[63]

The $Ca_5Sr_5(PO_4)_6F_2$ structure exhibits (statistical) disorder on the occupation of Ca1/Sr1 (65/35%) and Ca2/Sr2 (40/60%) sites, respectively (see Figure SI-1a). In agreement with previous results, strontium preferentially substitutes calcium into the seven-fold coordinated Ca2 calcium site close to the fluoride anions.[64] For the following calculation, the unit cell was doubled in the *c* direction and occupations chosen to obtain the global formula: $Ca1_5Ca2_5Sr1_3Sr2_7(PO_4)_{12}F_4$. The GIPAW calculated data for Sr1 (×3), Sr2 (×7) and P (×12) are given in Table SI4. For $Pb_{10}(VO_4)_6I_2$, two structures were calculated. The first one exhibits site occupancies of 1 for all atoms,[65] corresponding to the iodine in (0,0,0) position in the unit cell (space group P63/m with a = 10.4429(3) Å and c = 7.4865(2) Å). In order to further analyze the impact of iodine positions on the computed quadrupolar parameters, NMR parameters were also calculated for $Pb_{9.85}(VO_4)_6I_{1.7}$. Such a formula can be understood as: $Pb_{(10-x)}(VO_4)_6(PO_4)_0I_{(2-2x)}$ with $x = 0.15$ (see the general formula above). In this case, it was not possible to respect the occupation of the various sites[66] and unit cells with $Pb_{10}(VO_4)_6I_2$ stoichiometry were obtained by selection of atomic positions among those possible from a crystallographic point of view. Two of them were selected and are referenced as *Structure 1* and *Structure 2* in Table SI4. It should be noticed that in both cases, the iodine atoms were slightly shifted from the (0,0,0) position leading to two inequivalent positions in the unit cell (I1 and I2) (Table SI4).

Results and Discussion

BRAIN CP applied to "strong" half-integer quadrupolar nuclei: the case study of ^{87}Sr

As stated in the Introduction, ^{87}Sr is a rarely studied NMR-active nucleus. This can be undoubtedly related to the strong quadrupolar moment of ^{87}Sr leading to highly broadened lines even at the highest magnetic fields available (here, 20 T). In a recent contribution, we have also demonstrated that recording ^{87}Sr DFS WURST QCPMG NMR spectra was more complicated in the case of OH^- and/or H_2O containing derivative.[9] As a representative example, the spectrum of belovite, $Sr_{10}(PO_4)_6(OH)_2$, could not be obtained despite full optimization of the experimental parameters. The same problem is illustrated here by looking at strontium pyrophosphates including amorphous/crystallized and hydrated/non hydrated samples (Figure 1). The ^{87}Sr NMR spectrum of crystalline $Sr_2P_2O_7$ was characterized by the superposition of two second-order quadrupolar broadened lineshapes (Figure 1A*/*). These components were easily distinguished by significant differences in $C_Q(^{87}Sr)$, whereas $\delta_{iso}(^{87}Sr)$ *was not* a relevant parameter (as already mentioned in the literature[9,16]). The simulated parameters were in rather good agreement with computed data obtained from first principles GIPAW computations[9] (see Table 1 and Figure SI-4 for ^{31}P MAS NMR data). More precisely, one notes that the computed $\eta_Q(^{87}Sr)$ parameters are in very good agreement with the experimental data for both sites, Sr1 and Sr2. The same observation holds for $C_Q(^{87}Sr)$ in the case of Sr2, whereas $C_Q(^{87}Sr)$ for Sr1 is overestimated (in absolute value). At this stage, it remains difficult to explain such observation. Drastic changes in signal to noise ratio were observed in the case of

amorphous *hydrated* pyrophosphate ($Sr_2P_2O_7.4H_2O$) (Figure 1B/). Despite the longer experimental time (7 h), almost no spikelets were obtained. Upon heat treatment of this sample at 220° C, the intensity of the signal increased clearly demonstrating the negative influence of the water molecules on the ^{87}Sr detection (Figure 1C/). It follows that ^{87}Sr and ^{1}H nuclei play an intricate role which has to be kept in mind for the set-up of BRAIN CP experiments. Interestingly, the presence of other abundant nuclei with high magnetogyric ratio such as ^{19}F (representing therefore a spin bath as in the case of protons) did not hinder the acquisition of ^{87}Sr DFS WURST QCPMG, as demonstrated in the case of *non-hydrated* non-protonated $Sr(PO_3F)$ and $Ca_5Sr_5(PO_4)_6F_2$ (Figures 1D/ and SI-4, respectively). This is a clear difference compared to hydroxylated counterparts like $SrHPO_4$ and $Sr_{10}(PO_4)_6(OH)_2$, for which no ^{87}Sr NMR signal could be observed. In the particular case of $Ca_5Sr_5(PO_4)_6F_2$ in *natural abundance*, the limited wt% of Sr in the structure leads to intrinsic low sensitivity (see Figure SI-4). Clearly, much longer acquisition time should be necessary for relevant comparison with GIPAW computed data. For completeness of the study, the comparison of experimental and GIPAW computed quadrupolar parameters for $Sr(PO_3F)$ is presented in Table 1. As already observed for Sr1 in $Sr_2P_2O_7$ (see above), $C_Q(^{87}Sr)$ is again overestimated in the case of $Sr(PO_3F)$ though its order of magnitude is correct (indeed, $C_Q(^{87}Sr)$ values can reach huge values, up to ~ 80 MHz[9,16]).

The careful set-up and complete optimization of the $^{1}H \rightarrow {}^{87}Sr$ CP/ BRAIN CP experiments were performed starting from strontium malonate, $*Sr(CH_2(COO)_2$ (*labeled* in strontium-87). Such a derivative was previously characterized by ^{87}Sr DFS WURST QCPMG NMR, exhibiting a unique second-order quadrupolar broadened lineshape[9] (Figure 2A/). Here, a unique offset was sufficient to correctly excite the whole spectrum (~ 350 kHz). This was obviously not the case for the standard CP experiment (Figure 2B/) involving square pulses on both ^{1}H and ^{87}Sr channels. The excited bandwidth was strongly reduced (~ 43 kHz). The implementation and optimization of the BRAIN CP scheme led to a very large increase in the band excitation (~ 110 kHz) (Figure 2C/). With a single offset, the characteristic singularities of the lineshape were quite clearly observed. It followed that the number of necessary offsets for the VOCS BRAIN CP experiment was restricted to only six (insert of the Figure 2). At this stage, we mention two important points: *(i)* as $T_1(^{1}H)$ are usually much longer than $T_1(^{87}Sr)$, a flip back of the ^{1}H magnetization[67] was implemented in order to recycle it more efficiently and enhance the sensitivity of the experiment (this point will be stressed below in the case of *non-labeled* strontium malonate, $Sr(CH_2(COO)_2)$, *(ii)* looking carefully at the summed BRAIN CP spectrum in the insert of Figure 2, the most deshielded part of the spectrum (marked by a vertical arrow) is underestimated. In order to retrieve this "lost intensity", we tried to optimize the number of offsets, the power level of the proton channel, the type of experiment (CP *vs* BRAIN CP) and the contact time, t_{CP} (see Figure SI-5). All options failed. This observation demonstrates that only *slightly* distorted lineshapes can be observed by using VOCS CP/BRAIN CP experiments in the case of quadrupolar nuclei.

The impact of $T_1(^{1}H)$ (>> $T_1(^{87}Sr)$) was crucial when turning to *natural abundance* strontium derivatives such as strontium malonate (Figure SI-6). Using a unique offset, an overnight acquisition was necessary to obtain a reasonable signal to noise ratio. It is worth noting that at this stage, we did not try to improve the signal by post-processing techniques, more precisely by mathematical treatment of individual echoes in the acquisition time.

All in all, ^{87}Sr BRAIN CP WURST QCPMG experiment was carefully implemented using labeled strontium malonate as a suitable reference compound. Such an experiment seemed rather robust apart from slight distortions of the lineshapes. The main drawback of the sequence remained the negative effects of long $T_1(^{1}H)$. Such drawback can occur even in the case of *labeled* samples, as observed for strontium phenylboronate, $*Sr(C_6H_5B(OH)_3)_2.H_2O$ (see Figure SI-7). In this particular case, a relaxation delay of ~ 10 s was found to be the minimum value. While the use of a flipback pulse on the ^{1}H compensates for this issue, another approach to circumvent such relaxation problem could be to add a very small amount of paramagnetic species in the material (e.g. Cu^{2+}, Ni^{2+}…)[68] in order to strongly shorten $T_1(^{1}H)$ values and make the recycle delay competitive with the one used for direct WURST QCPMG acquisition. In this case, we stress that the amount of paramagnetic species will have to be optimized in order to avoid severe paramagnetic relaxation and keep a reasonable number of echoes in the QCPMG experiment. We mention also that other abundant nuclei (such as ^{19}F) could act as an efficient spin bath for CP transfer to ^{87}Sr. Such an experiment could be of prime importance for the discrimination of the two Sr sites in the $Ca_5Sr_5(PO_4)_6F_2$ structure, based on the $^{19}F \rightarrow {}^{87}Sr$ heteronuclear dipolar coupling (indeed, the structure is characterized by two independent Sr positions, one being located closer to the F atoms). Such an approach was successfully applied to the study of tin oxo-clusters by $^{19}F \rightarrow {}^{119}Sn$ BRAIN CP (see below).

^{127}I: a local spy for disorder characterization in iodine substituted apatite

The ^{127}I quadrupolar coupling constants can vary from ~ 0 to ~ 200 MHz even in the case of iodide salts.[39a] In Figure SI-8, the ^{127}I wideline spectra of PbI_2 and CdI_2 are presented and illustrate the

strong variation of $C_Q(^{127}I)$ from one compound to the other (see Table 1). For the largest constants, the VOCS WURST QCPMG approach was clearly advantageous in terms of sensitivity (DFS was not necessary here). This is particularly visible in the case of CdI_2, as the full lineshape, which is ~ 2 MHz wide, could be recorded in only 40 minutes.

The ^{127}I VOCS WURST QCPMG spectrum of $Pb_{10}(VO_4)_6I_2$ is presented in Figure 3A/ (sum of three offsets). The crystallographic structure of this apatite-like structure contains a single iodide environment at (0,0,0) position, and the lineshape could indeed be simulated by a single set of quadrupolar and isotropic chemical shift parameters. The ^{127}I GIPAW computed parameters are presented in Table 1. The agreement between the calculated and experimental $\delta_{iso.}(^{127}I)$ is excellent whereas $C_Q(^{127}I)$ is somehow underestimated. Moreover, the CSA is estimated to ~ –350 ppm in agreement with data published in the literature for other metal iodides and their hydrates.[39a] As already mentioned by Bryce *et al*.[39a], small displacements of iodine atoms in the cell have a tremendous impact on the calculated values of $C_Q(^{127}I)$. These authors estimated that displacements of ~ ± 0.07 Å could lead to variations of $\Delta C_Q(^{127}I) \sim 120$ MHz in the case of MgI_2 and CaI_2. The same computational trend is observed for $Pb_{10}(VO_4)_6I_2$. In Table SI4, small variations of the x/a, y/b and z/c parameters for I1 and I2 (< 0.03 Å) led to very strong overestimations of $C_Q(^{127}I)$ and a net degradation of $\delta_{iso.}(^{127}I)$. In other words, ^{127}I is extremely sensitive to local environment and can act as a useful tool for NMR crystallography. In the case of $Pb_{10}(VO_4)_6I_2$, the crystallographic structure given in ref 65 seems therefore of very good quality from this particular point of view.

Related apatitic phases synthesized using $Pb_3(VO_4)_{1.6}(PO_4)_{1.2}$ and PbI_2 (following various protocols – see the Experimental Section, samples **1** to **5**) were also characterized by ^{127}I WURST QCPMG NMR (Figures 3B/ to F/). We recall here that the general formula for these compounds is $Pb_{(10-x)}(VO_4)_{4.8}(PO_4)_{1.2}I_{(2-2x)}$ and that their XRD powder patterns are very similar (see Figure SI-2). It follows that no clear structural distinction between the samples could be established. As already mentioned in the Experimental Section, it was particularly difficult to estimate the small variations of the "x" parameter. At first glance, all ^{127}I NMR spectra were globally comparable, involving similar quadrupolar parameters. However, looking more carefully at each ^{127}I individual line, and using the lineshape of $Pb_{10}(VO_4)_6I_2$ as a guideline (light green dashed line), two groups of spectra can be distinguished. The spectra of samples **1** and **2** were quite comparable to that of $Pb_{10}(VO_4)_6I_2$. However, the spectra related to samples **3** to **5** were different, especially in the more shielded region (green vertical arrow). In the latter cases, a "smoother" asymmetric line was observed. It could correspond to a distribution of quadrupolar parameters ($C_Q(^{129}I)$) directly related to non-stoichiometry in the general formula, $Pb_{(10-x)}(VO_4)_{4.8}(PO_4)_{1.2}I_{(2-2x)}$. A simulation using the Czjzek model[69, 70] and an explicit C_Q distribution is presented in Figure 3D/ (red line). Very interestingly, we observe that the more disordered samples correspond to those obtained at the highest temperature (**4**) and starting with the most deficient compositions in PbI_2 (**3** and **5**). It follows that the ^{127}I lineshape reflects the local order/disorder around iodine crystallographic sites. At this stage, we stress on the fact that the above cited distributions should correspond to minute variations of chemical environments (involving most probably second- or even third neighbors) as $C_Q(^{129}I)$ is an ultra-sensitive parameter (see above and Table SI4). Such detailed insight into the iodine local environment had never been achieved for these materials.

Spectral editing by $^1H/^{19}F \rightarrow {}^{119}Sn$ BRAIN CP: site characterization and anions proximities

The ^{119}Sn WURST CPMG NMR spectrum of **$(BuSn)_{12}(OH)_2$** (under high power ^1H decoupling) was first recorded (Figure 4A/). As already stated in the Experimental Section, all parameters related to the acquisition were fully optimized. Under such optimized conditions, a unique offset was sufficient to acquire the whole lineshape (~ 250 kHz). As expected from ^{119}Sn fast MAS NMR experiments, the spectrum could be interpreted by considering two types of Sn atoms: six 5 fold coordinated Sn or $CSnO_4$, (deshielded contribution), and six 6 fold coordinated Sn or $CSnO_5$ (shielded contribution) (insert in Figure 4). In **$(BuSn)_{12}(OH)_2$**, all Sn atoms are linked to a butyl group ($-C_4H_9$). Moreover, the 6 fold coordinated Sn atoms are involved in one Sn–OH–Sn bond. Ribot *et al*.[25,26,27] have demonstrated previously that under fast MAS conditions, subtle variations of $\delta_{iso}(^{119}Sn)$ had been observed with $<\delta_{iso}(^{119}Sn)> \sim -279$ and $<\delta_{iso}(^{119}Sn)> \sim -467$ ppm for $CSnO_4$ and $CSnO_5$, respectively. For $CSnO_5$ species, variations of $\delta_{iso}(^{119}Sn)$ up to ~ 35 ppm could be observed. From Figure 4, it seemed obvious that *averaged* values of the NMR parameters ($\delta_{iso}(^{119}Sn)$, $\delta_{CSA}(^{119}Sn)$, $\eta_{CSA}(^{119}Sn)$) could be solely extracted by simulating the spectra, as the necessary resolution was not achieved under static CPMG conditions. The simulated parameters corresponding to Figure 4B*/* are given in Table 1. Quantitatively, the ratio between the areas of the two components was maintained to be ~ 1 (in agreement with the crystallographic data). All simulated values were comparable to those already observed for **$(BuSn)_{12}$** derivatives under ^{119}Sn fast MAS.[25,26]

$(BuSn)_{12}(OH)_2$ was further studied by CP and BRAIN CP CPMG experiments. This sample was interesting in terms of *spectral editing* as $CSnO_4$ and $CSnO_5$ sites are actually characterized by different

chemical environments (with OH^- groups closer to $CSnO_5$ sites). In other words, the $^1H \rightarrow {}^{119}Sn$ heteronuclear dipolar couplings are stronger for $CSnO_5$ (when compared to $CSnO_6$) and should lead to an overestimation of the $CSnO_5$ sites in a CP experiment. First, the efficiency of the BRAIN approach (over the standard CP scheme with rectangular pulses) was clearly demonstrated (see Figure SI-9). Here a unique offset was used for comparison. It is obvious that the excitation band obtained under BRAIN CP conditions is much broader than that obtained under standard CP (roughly by a factor of ~ 2). Moreover, it is interesting to note that a unique BRAIN CP excitation led to a distorted lineshape when compared to Figure 4. In other words, the VOCS (BRAIN CP) was necessary here. The result of the VOCS BRAIN CP approach applied to $(BuSn)_{12}(OH)_2$ is presented in Figure 5A*I*. As expected, the component related to $CSnO_5$ was overestimated in good agreement with the above cited analysis of the ^1H–^{119}Sn heteronuclear dipolar couplings. In Figure SI-10, the effect of the cross-polarization contact time (t_{CP}), was carefully analyzed, varying from 4 to 16 ms. As shown in the Experimental Section, the WURST shape (during t_{CP}) was carefully computed and optimized in each case. Whatever the contact time, the overestimation of the $CSnO_5$ component was obvious. Moreover, we note that no significant evolution of the spectra occurred during the variation of t_{CP} demonstrating the robustness of the BRAIN CP scheme.

Related **(BuSn)$_{12}$**SO_4 and **(BuSn)$_{12}$**$(O_3SCF_3)_2$ phases were studied by ^{119}Sn BRAIN CP as well (see Figures 5B/ and C/, respectively). It is well established that all **(BuSn)$_{12}$** tin oxo-cores exhibit the same global structure with six hydroxyl groups in close vicinity to the six $CSnO_5$ sites. The ^{119}Sn BRAIN CP spectra were comparable to **(BuSn)$_{12}$**$(OH)_2$, both in terms of CSA parameters for $CSnO_4$ and $CSnO_5$ environments, and of relative intensities (with an overestimation of $CSnO_5$ sites). One notes that in the case of **(BuSn)$_{12}$**$(O_3SCF_3)_2$, CSA of $CSnO_5$ could be estimated to be ~ –300 ppm. Such values remained in agreement with those published previously.[25,26,27]

In order to further investigate the structure of **(BuSn)$_{12}$**$(O_3SCF_3)_2$, $^{19}F \rightarrow {}^{119}Sn$ BRAIN CP MAS experiments were implemented. The ^{19}F MAS NMR spectrum is presented as an insert in Figure 6. A unique isotropic signal ($\delta_{iso}(^{19}F)$ = –78.0 ppm) was observed with a set of spinning sidebands characterized by $\delta_{CSA}(^{19}F)$ = 42 ppm (±3) and $\eta_{CSA}(^{19}F)$ = 0.20 (±0.15). The corresponding static lineshape extended over ~ 50 kHz. From a structural point of view, the $CF_3SO_3^-$ anions can adopt: *(i)* a terminal position (see insert 1 in Figure 6) involving three OH…O hydrogen bonds. Such a configuration is usually observed in solution. *(ii)* A bridging position (see insert 2 in Figure 6) linking two distinct **(BuSn)$_{12}$** oxo-clusters with two OH…O hydrogen bonds with one oxo-cluster and one hydrogen bond with a distinct oxo-cluster. In case *(i)*, the minimum $d_{F\text{-}Sn}$ distances are clearly different when considering $CSnO_4$ and $CSnO_5$ (9.3 and 6.3 Å, respectively). Using the following formula for the estimation of the ^{19}F–^{119}Sn heteronuclear dipolar constant, D_{F-Sn} (in kHz):[71]

$$D_{F-Sn} = (122\ kHz)\frac{(|\gamma_{^{119}Sn}|/\gamma_{^1H})(\gamma_{^{19}F}/\gamma_{^1H})}{(d_{F-Sn})^3},$$

where γ corresponds to the magnetogyric ratio of the nucleus and $d_{F\text{-}Sn}$ is given in Å, one obtains $D_{F\text{-}Sn}$ ~ 50 and 170 Hz for $CSnO_4$ and $CSnO_5$, respectively. In other words, $CSnO_5$ sites should be overestimated during the CP transfer from the ^{19}F spin bath. On the contrary, in case *(ii)*, $d_{F\text{-}Sn}$ distances are comparable for $CSnO_4$ and $CSnO_5$ (~ 5 Å for both) leading to $D_{F\text{-}Sn}$ ~ 340 Hz. Consequently, the order of magnitude of the dipolar coupling is comparable for both sites. As shown in Figure 6, both $CSnO_4$ and $CSnO_5$ sites were each detected to a similar extent in agreement with the structural assumption *(ii)* (bridging $CF_3SO_3^-$ anions). Such bridging character of the anions has been systematically observed in the solid state structure of various $\{(BuSn)_{12}O_{14}(OH)_6\}^{2+}$ derivatives.[25,26,30] This is the first time that such an assumption was demonstrated for a structure for which *no X-ray diffraction data* exists. At this stage, we mention that the $^{19}F \rightarrow {}^{119}Sn$ BRAIN CP efficiency is much lower when compared to $^1H \rightarrow {}^{119}Sn$ BRAIN CP. This observation could be related to the lower $\gamma_{^{19}F}$, the much shorter $d_{H\text{-}Sn}$ distances when compared to $d_{F\text{-}Sn}$ and the higher ^1H "content" of the **(BuSn)$_{12}$** oxo-cluster leading to much more efficient spin diffusion among protons. For the optimization of the experiment, the following trends were followed (compared to $^1H \rightarrow {}^{119}Sn$ BRAIN CP): a significant increase of the number of scans, the increase of the contact time (up to 32 ms), and the increase of the spikelet separation (CPMG) for optimized experimental time.

Finally, another organotin derived oxo-core was studied by $^1H \rightarrow {}^{119}Sn$ BRAIN CP, namely **(BuSn)$_6$**$(O_2CC_6H_4NH_2)_6$, in which six $CSnO_5$ sites are present. The structure of the cluster is presented in Figure 7. ^{119}Sn fast MAS experiments (not shown here) led to observation of two isotropic lines (in a 2:1 ratio) with very similar CSA parameters, namely $\delta_{CSA}(^{119}Sn)$ ~ –375 ppm and $\eta_{CSA}(^{119}Sn)$ ~ 0.25. As mentioned above in the case of **(BuSn)$_{12}$** clusters, the analysis of the static $^1H \rightarrow {}^{119}Sn$ BRAIN CP spectrum led to averaged values of the CSA parameters (see Table 1) which were indeed comparable to data obtained by ^{119}Sn fast MAS. Nevertheless, a slight discrepancy between experimental and simulated $\eta_{CSA}(^{119}Sn)$ was observed, confirming that lineshape distortions can occur using BRAIN CP-type sequences.

Conclusions

In this contribution, we have demonstrated that advanced solid state NMR techniques could be valuable tools of investigation for materials involving strontium, iodine and tin. These materials are of highest interest as potential biomaterials, inorganic matrices for the immobilization of radioactive nuclides and building blocks for the synthesis of tailored functional nanostructured architectures. The common feature of the targeted nuclei is related to the strong anisotropy associated to the involved NMR interactions, here quadrupolar and/or CSA. In particular, we have applied for the first time the BRAIN CP approach to a non-integer quadrupolar nucleus, namely ^{87}Sr (I = 9/2). We have stressed on the experimental conditions leading to the less distorted lineshapes. In the case of ^{127}I, subtle variations of the spectra were interpreted in terms of C_Q distributions. ^{127}I GIPAW calculations demonstrated also that the $C_Q(^{127}I)$ parameter was highly sensitive to minute variations of chemical environments acting therefore as a pertinent descriptor in NMR crystallography. Finally, the $^{1}H/^{19}F \rightarrow {}^{119}Sn$ BRAIN CP approach was successfully applied to the *spectral editing* of spectra in terms of $^{1}H/^{19}F–^{119}Sn$ dipolar interactions. This was of particular help in the case of derivatives without any available crystallographic structure. Overall, it is believed that the work presented here will help expand the range of applications of wideline acquisition solid state NMR methods to solve structural questions in a variety of materials.

Acknowledgements

The French/UK CNRS PICS project QMAT is acknowledged. The UK 850 MHz solid-state NMR Facility used in this research was funded by EPSRC and BBSRC, as well as the University of Warwick including via part funding through Birmingham Science City Advanced Materials Projects 1 and 2 supported by Advantage West Midlands (AWM) and the European Regional Development Fund (ERDF). NMR spectroscopic calculations were performed using HPC resources from GENCI-IDRIS (Grant 2016-097535). Financial support from the TGIR-RMN-THC Fr3050 CNRS for conducting the research is gratefully acknowledged. More specifically, DL and CB warmly thank Franck Fayon for helpful discussions on both instrumental and experimental topics related to WURST QCPMG experiments.

Keywords: BRAIN CP • WURST QCPMG• ^{87}Sr, ^{119}Sn, ^{127}I wideline NMR • Strontium malonate/boronate • Iodo/fluoroapatite • Tin oxo-clusters.

Table 1. Experimental (extracted from simulations of NMR spectra using DMFit[63]) and GIPAW[61] computed values (in *italics*) for CSA and quadrupolar parameters (when present) for $Sr_2P_2O_7$, $Sr(PO_3F)$, Sr-phenylboronate, Sr-malonate, $Ca_5Sr_5(PO_4)_6F_2$, PbI_2, CdI_2, $Pb_{10}(VO_4)_6I_2$, **(BuSn)$_{12}$**$(OH)_2$, and **(BuSn)$_6$**$(O_2CC_6H_4NH_2)_6$. Estimated error bars are given in parentheses. Only absolute value of C_Q can be obtained experimentally whereas its sign can be extracted from GIPAW calculations.

compound	δ_{iso} (ppm)	δ_{CSA} (ppm)	η_{CSA}	C_Q (MHz)	η_Q
$Sr_2P_2O_7$					
Sr1	0 (±75)	–	–	17.00 (±0.50)	0.20 (±0.15)
	–34.2	*–21.3*	*0.44*	*–21.35*	*0.18*
Sr2	80 (±80)	–	–	33.00 (±0.75)	0.20 (±0.10)
	37.7	*70.0*	*0.70*	*–34,00*	*0.20*
P1	–7.04 (±0.05)	60.8 (±1.0)	0.36 (±0.05)	–	–
	–4.35	*67.53*	*0.29*	–	–
P2	–9.13 (±0.05)	71.0 (±1.0)	0.19 (±0.05)	–	–
	–7.10	*78.86*	*0.14*	–	–
$Sr(PO_3)F$					
Sr	100 (±150)	–	–	31.5 (±1.5)	0.9 (±0.1)
	–4.4	*–55.0*	*0.61*	*–37.40*	*0.84*
P	–	–	–	–	–
	1.3	*95.9*	*0.20*	–	–
Sr-phenyl-boronate					
Sr	50 (±60) [b]	–	–	20.20	0.25
	37.7	*–27.1*	*0.43*	*21.78*	*0.54*
Sr-malonate					
Sr	0 (±60) [b]	–	–	31.50	0.80
	–16.8	*40.3*	*0.83*	*28.13*	*1.00*
$Ca_5Sr_5(PO_4)_6F_2$					
Sr1	–	–	–	–	–
	108.3 [c]	*–76.9*	*0.02*	*–50.07*	*0.01*
Sr2	–	–	–	–	–
	72.9	*63.3*	*0.51*	*–35.78*	*0.90*
P [d]	–	–	–	–	–
	–0.5	*6.5*	*0.51*	–	–
PbI_2					
I	325 (±4) [e]	–	–	21.00 (±0.2)	0.05 (±0.05)
	357.8	*–27.7*	*0.04*	*–20.78*	*0.00*
CdI_2					
I	1450 (±50) [e]	–	–	96.0 (±0.5)	0.05 (±0.05)
	1394.3	*195.5*	*0.00*	*89.29*	*0.00*
$Pb_{10}(VO_4)_6I_2$					
I	1565 (±50)	–	–	35.00 (±0.75)	0.90 (±0.10)
	1572.9	*-345.6*	*0.00*	*–22.38*	*0.00*
(BuSn)$_{12}$ $(OH)_2$					
Sn	–280 (±10) [f]	–300 (±25) [f]	0.20 (±0.15) [f]	–	–
	–475 (±15) [g]	–250 (±25) [g]	0.20 (±0.15) [g]	–	–
(BuSn)$_6$$(O_2CC_6H_4NH_2)_6$					
Sn	–486 (±10) [g]	–350 (±10) [g]	0.05 (±0.05) [g]	–	–

[a] the computed data in *italics* correspond to the $Sr_2P_2O_7$ α-phase. [b] experimental data taken from ref. 9. [c] average of three almost identical values for Sr1 and seven almost identical values for Sr2. [d] average over all P sites. [e] for PbI_2 and CdI_2 data, see also ref. 39a. [f] averaged values for all $CSnO_4$ sites. [g] averaged values for all $CSnO_5$ sites.

Figure 1. A/ ^{87}Sr DFS WURST QCPMG spectrum (Exp.) of $Sr_2P_2O_7$ (one offset, experimental time ~ 4h). Simulation of the spectrum (Sim.) using two quadrupolar lineshapes (central transitions, CT, in orange and green). The corresponding NMR parameters are given in Table 1. Some contribution of the satellite transitions (ST) was detected as well, but not taken into account in the simulation. **B/** ^{87}Sr DFS WURST QCPMG spectrum (Exp.) of amorphous $Sr_2P_2O_7.4H_2O$ (one offset, experimental time ~ 7h). **C/** ^{87}Sr DFS WURST QCPMG spectrum (Exp.) of amorphous $Sr_2P_2O_7.4H_2O$ *after heat treatment at 220°C* (one offset, experimental time ~ 14 h). **D/**: ^{87}Sr DFS WURST QCPMG spectrum (Exp.) of $Sr(PO_3F)$ (4 offsets, experimental time ~ 8h). Simulation of the spectrum (Sim.) using a single quadrupolar lineshape in agreement with crystallographic data.[72]

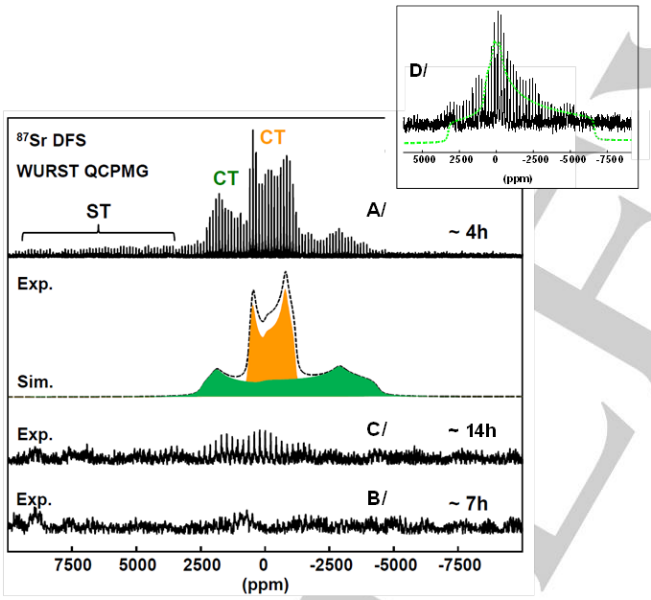

Figure 2. A/ ^{87}Sr DFS WURST QCPMG spectrum of ^{87}Sr *labeled* Sr-malonate (one offset). The simulated green dashed line corresponds to the NMR parameters given in Table 1. **B/** and **C/** ^{1}H/^{87}Sr CP and BRAIN CP WURST QCPMG spectra (with flip back of the ^{1}H magnetization) of ^{87}Sr *labeled* Sr-malonate, respectively (one offset). The red horizontal arrows show the excited regions of the spectra. **Insert**: direct: ^{87}Sr DFS WURST QCPMG spectrum of ^{87}Sr *labeled* Sr-malonate (one offset). BRAIN CP: ^{1}H → ^{87}Sr VOCS BRAIN CP WURST QCPMG spectrum (with flip back of the ^{1}H magnetization) of ^{87}Sr *labeled* Sr-malonate (6 offsets). The red vertical arrow indicates the *underestimation* of the most deshielded part of the spectrum under BRAIN CP conditions.

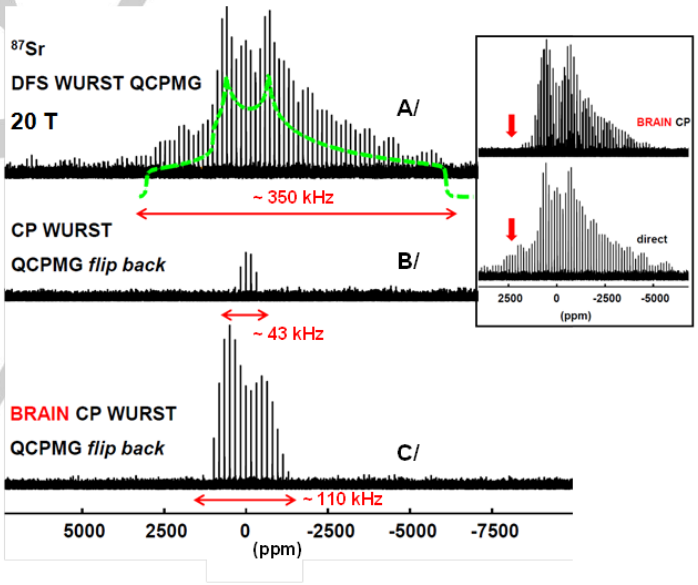

Figure 3. A/ ^{127}I VOCS WURST QCPMG spectrum of $Pb_{10}(VO_4)_6I_2$ (3 offsets). Green dashed line: simulation of the sum spectrum with a single set of NMR parameters (see Table 1). **B/** to **F/** ^{127}I VOCS WURST QCPMG spectra of $Pb_{(10-x)}(VO_4)_{4.8}(PO_4)_{1.2}I_{(2-2x)}$, samples **1** to **5** (see the Experimental Section for the synthesis protocols) (3 offsets as well). The green dashed line is used here as a guideline for the eyes. The green vertical arrow shows the main differences between the simulated lineshape corresponding to $Pb_{10}(VO_4)_6I_2$ and the spectra of samples **3** to **5**. Red solid line: Czjzek model[69,70] with the following parameters: isotropic average value: 1645 ppm, no isotropic chemical shift Gaussian distribution, quadrupolar coupling of the distribution: 37.1 MHz (Czjzek module in DMFit), critical exponent: d = 5.

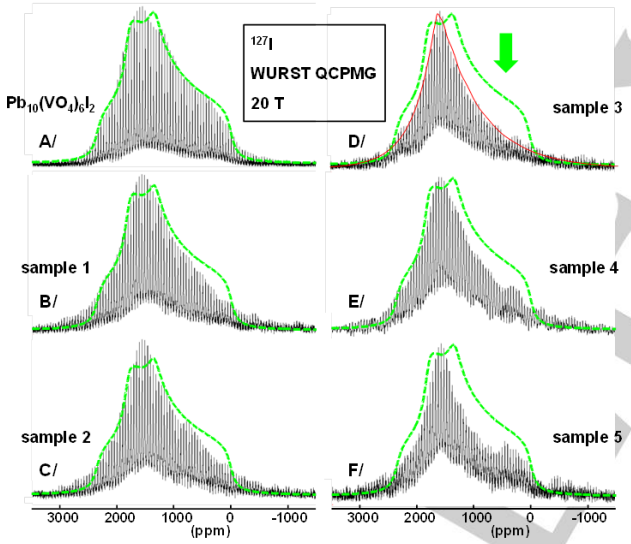

Figure 4. A/ ^{119}Sn WURST CPMG spectrum of **$(BuSn)_{12}(OH)_2$** (one offset). **B/** Simulation of the experimental spectrum using two CSA lineshapes (parameters are given in Table 1) for $CSnO_4$ (5 fold coordinated) and $CSnO_5$ (6 fold coordinated) tin sites. **Insert**: schematic representation of the **$(BuSn)_{12}$** oxo-cluster. Green: $CSnO_4$, blue: $CSnO_5$, light blue: C (only the first carbon atom of each butyl chain is represented for better clarity), red: oxygen, black: H (from OH groups linked to $CSnO_5$).

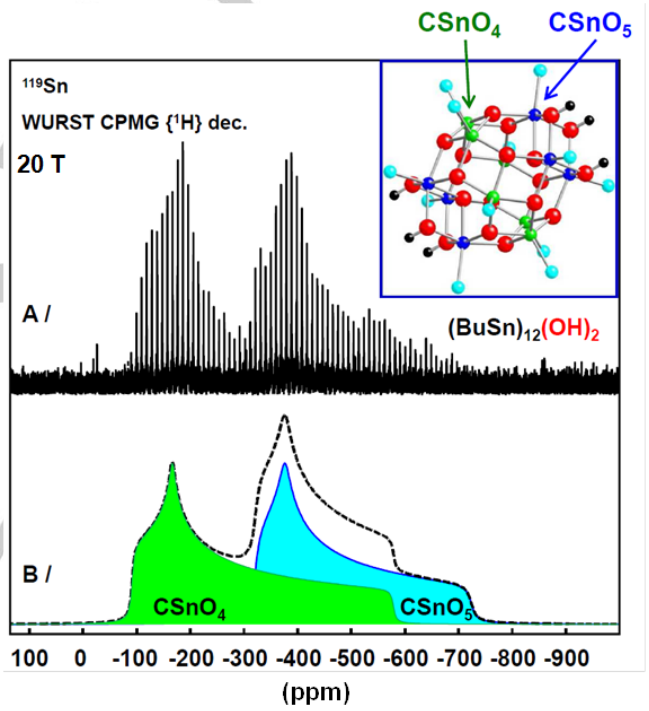

Figure 5. $^{1}H \rightarrow {}^{119}Sn$ VOCS BRAIN CP WURST CPMG spectra of **A/ $(BuSn)_{12}(OH)_2$** (3 offsets), **B/ $(BuSn)_{12}SO_4$** (5 offsets), **C/ $(BuSn)_{12}(O_3SCF_3)_2$** (5 offsets). $CSnO_4$ and $CSnO_5$ regions are indicated by vertical grey arrows. The contact time, t_{CP}, is fixed (8 ms). **Insert:** schematic representation of the **$(BuSn)_{12}$** oxo-cluster (the code of colors is given in Figure 4).

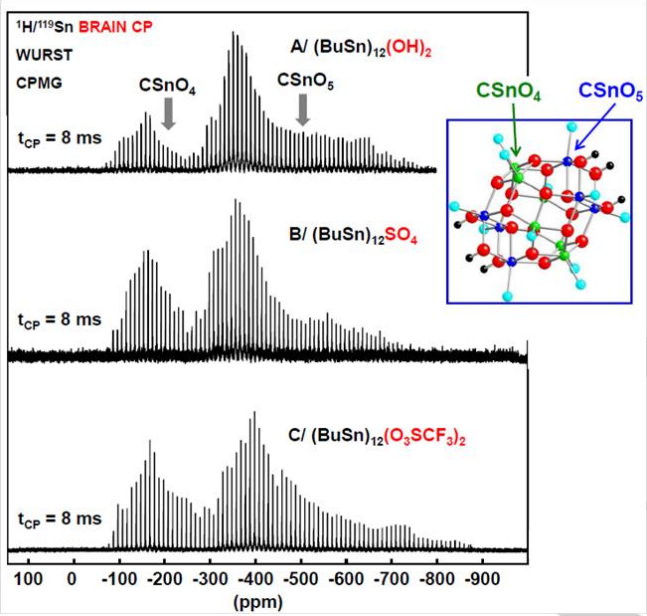

Figure 6. $^{19}F \rightarrow {}^{119}Sn$ BRAIN CP WURST CPMG spectra of **$(BuSn)_{12}(O_3SCF_3)_2$** (2 offsets). $CSnO_4$ and $CSnO_5$ regions are indicated by vertical grey arrows. **Insert 1**: schematic representation of a single **$(BuSn)_{12}$** oxo-cluster capped by two *non-bridging* $CF_3SO_3^-$ anions. **Insert 2**: schematic representation of two **$(BuSn)_{12}$** oxo-clusters linked by two *bridging* $CF_3SO_3^-$ anions (the code of colors is given in Figure 4, pink: fluorine). **Insert**: ^{19}F MAS spectra (experimental, black solid line, and simulated, black dashed line). The width of the corresponding ^{19}F static spectrum is ~ 50 kHz.

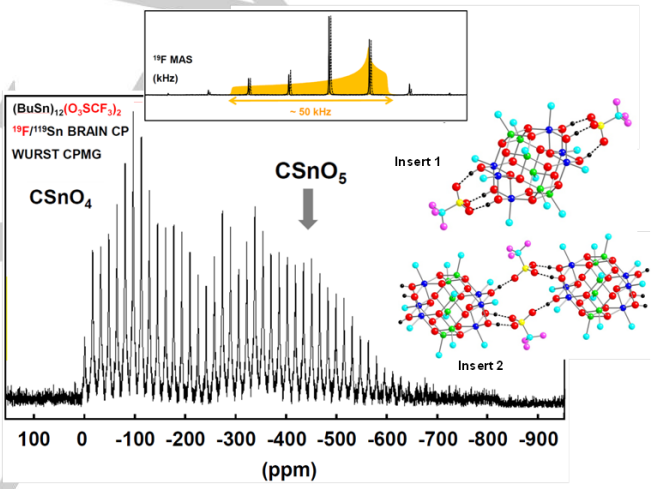

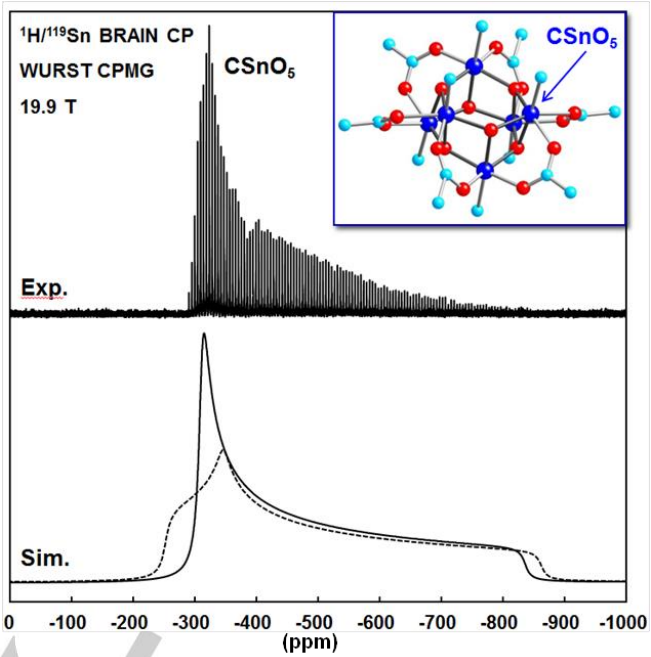

Figure 7. ^{1}H → ^{119}Sn VOCS BRAIN CP WURST CPMG spectrum of **(BuSn)$_6$**($O_2CC_6H_4NH_2$)$_6$ (Exp.) (3 offsets). Sim.: solid line: best simulation of the experimental lineshape. Dashed line: calculated static spectrum starting from ^{119}Sn MAS data (see main text).

FULL PAPER

Full experimental details are given for the robust set up of ^{87}Sr,^{119}Sn and ^{127}I VOCS WURST (Q)CPMG BRAIN CP NMR experiments and their application to the detailed study of Sr-derived materials, nanometric tin oxo-cores and iodoapatites.

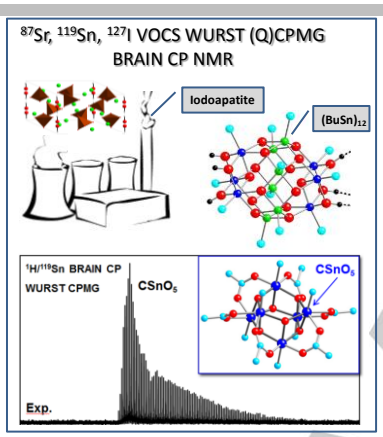

*Author(s), Corresponding Author(s)**

Page No. – Page No.

Title

[1] C. Bonhomme, C. Gervais, D. Laurencin, *Prog. Nucl. Magn. Reson. Spectrosc*. **2014**, *77*, 1-48.
[2] C. Bonhomme, C. Gervais, F. Babonneau, C. Coelho, F. Pourpoint, T. Azaïs, S. E. Ashbrook, J. M. Griffin, J. R. Yates, F. Mauri, C. J. Pickard, *Chem. Rev.* **2012**, *112*, 5733-5779.
[3] T. Charpentier, *Solid State NMR* **2011**, *40*, 1-20.
[4] *NMR Crystallography*, R. K. Harris, R. E. Wasylishen, M. J. Duer, editors, Wiley, 2009 and references therein.
[5] R. W. Schurko, *Acc. Chem. Res*. **2013**, *46*, 1985-1995.
[6] *Multinuclear Solid-State NMR of Inorganic Materials*, K. J. D. Mackenzie, M. E. Smith, Pergamon Materials Series, Pergamon, 2002.
[7] R. W. Schurko, in *NMR of Quadrupolar Nuclei in Solids*, R. E. Wasylishen, S. E. Ashbrook, S. Wimperis, editors, Wiley, 2012 and references therein.
[8] P. J. Meunier, C. Roux, E. Seeman, S. Ortolani, J. E. Badurski, T. D. Spector, J. Cannata, A. Balogh, E. M. Lemmel, S. Pors-Nielsen *et al*., *New Engl. J. Med*. **2004**, *350*, 459-468.
[9] C. Bonhomme, C. Gervais, N. Folliet, F. Pourpoint, C. Coelho-Diogo, J. Lao, E. Jallot, J. Lacroix, J.-M. Nedelec, D. Iuga, J. V. Hanna, M. E. Smith, Y. Xiang, J. C. Du, D. Laurencin, *J. Am. Chem. Soc.* **2012**, *134*, 12611-12628.
[10] J. Braux, F. Velard, C. Guillaume, S. Bouthors, E. Jallot, J.-M. Nedelec, D. Laurent-Maquin, P. Laquerrière, *Acta Biomater*. **2011**, *7*, 2593–2603.
[11] S. Sriranganathan, N. Kanwal, K. A. Hing, R. G. Hill, *J. Mater. Science: Mater. in Medicine* **2016**, 27:39.
[12] K. Fujikura, N. Karpukhina, T. Kasuga, D. S. Brauer, R. G. Hill, R. V. Law *J. Mater. Chem*. **2012**, *22*, 7395-7402.
[13] J. Lao, E. Jallot, J.-M. Nedelec, *Chem. Mater.* **2008**, *20*, 4969-4973.
[14] D. Berthomieu, C. Gervais, G. Renaudin, M. Reinholdt, S. Sene, M. E. Smith, C. Bonhomme, D. Laurencin, *Eur. J. Inorg. Chem.* **2015**, *7*, 1182-1191.
[15] M. Reinholdt, J. Croissant, L. Di Carlo, D. Granier, P. Gaveau, S. Bégu, J.-M. Devoisselle, H. Mutin, M. E. Smith, C. Bonhomme, C. Gervais, A. van der Lee, D. Laurencin, *Inorg. Chem.* **2011**, *50*, 7802-7810.
[16] A. Faucher, V. V. Terskikh, E. Ye, G. M. Bernard, R. E. Wasylishen, *J. Phys Chem. A* **2015**, *119*, 11847-11861.
[17] G. M. Bowers, R. Ravella S. Komarneni, K. T. Mueller *J. Phys. Chem. B*, **2006**, *110*, 7159–7164.
[18] K. M. N. Burgess, Y. Xu, M. C. Leclerc, D. L. Bryce *Inorg. Chem.*, **2014,** 53, 552–561.

[19] D. L. Bryce, J. Viger-Gravel, *Top. Curr. Chem*. **2015**, *358*, 183-203.
[20] B. J. Riley, J. D. Vienna, D. M. Strachan, J.S. McCloy, J. L. Jerden, *J. Nucl. Mater*. **2016**, *470*, 307e326.
[21] S. Le Gallet, L. Campayo, E. Courtois, S. Hoffmann, Y. Grin, F. Bernard, F. Bart *J. Nucl. Mater*. **2010**, *400*, 251-256.

[22] L. Campayo, A. Grandjean, A. Coulon, R. Delorme, D. Vantelon, D. Laurencin *J. Mater. Chem*. **2011**, 21, 17609-17611.
[23] D. L. Bryce, C. M. Widdifield, R. P. Chapman, R. J. Attrell, Robert J., *Encyclopedia of NMR* **2012**, 1, 586-604 (Edited by Harris, Robin K.; Wasylishen, Roderick E.).
[24] a) L. P. Cruz, J.-M. Savariault, J. Rocha, J.-C. Jumas, J. D. Pedrosa de Jesus, *J. Solid State Chem*. **2001**, *156*, 349-354. b) S. K. Kulshreshtha, R. Sasikala, V. Sudarsan, *J. Mater. Chem*. **2001**, *11*, 930-935. c) A. Sebald, L. H. Merwin, W. A. Dollase, F. Seifert, *Phys. Chem. Minerals* **1990**, *17*, 9-16.
[25] F. Banse, F. Ribot, P. Tolédano, J. Maquet, C. Sanchez, *Inorg. Chem*. **1995**, *34*, 6371-6379.
[26] C. Eychenne-Baron, F. Ribot, N. Steunou, C. Sanchez, *Organometallics* **2000**, 19, 1940-1949.
[27] F. Ribot, C. Sanchez, R. Willem, J. C. Martins, M. Biesemans, *Inorg. Chem*. **1998**, *37*, 911-917.
[28] F. Ribot, C. Eychenne-Baron, C. Sanchez, *Phosphorus, Sulfur, and Silicon* **1999** *150-151*, 41-58.
[29] C. Sanchez, G.J.A.A. Soller-Illia, F. Ribot, T. Lalot, C.R. Mayer, V. Cabuil, *Chem. Mater.* **2001**, *13*, 3061-3083.
[30] F. Ribot, D. Veautier, S. Guillaudeu, T. Lalot, *J. Mater. Chem.* **2005**, *15*, 3973-3978.
[31] F. Ribot, A. Lafuma, C. Eychenne-Baron, C. Sanchez, *Adv. Mater.* **2002**, *14*, 1496-1499.
[32] F. Potier, A. Guinault, S. Delalande, C. Sanchez, F. Ribot, L. Rozes, *Poly. Chem.* **2014**, *5*, 4474-4479.
[33] A. Strachota, K. Rodzeń, F. Ribot, M. Trchova, M. Steinhart, L. Starovoytova, E. Pavlova, *Macromolecules* **2014**, *47*, 4266-4287.
[34] B. Wrackmeyer, E. Kupce, G. Kehr, A. Sebald, *Mag. Res. Chem*. **1992**, *30*, 964-968.
[35] A. Lycka, D. Micak, J. Holecek, M. Biesemans, J. C. Martins, R. Willem, *Organomet*. **2000**, *19*, 703-706.
[36] L. A. O'Dell, *Solid State NMR* **2013**, *55-66*, 28-41.
[37] D. Iuga, H. Schäfer, R. Verhagen, A. P. M. Kentgens, *J. Magn. Reson*. **2000**, *147*, 192-209.
[38] D. Massiot, I. Farnan, N. Gautier, D. Trumeau, A. Trokiner, J.-P. Coutures, *Solid State NMR* **1995**, *4*, 241-248.
[39] a) C .M. Widdifield, D. L. Bryce, *J. Phys. Chem. A* **2010**, *114*, 10810-10823. b) C. M. Widdifield, G. Cavallo, G. A. Facey, T. Pilati, J. Lin, P. Metrangolo, G. Resnati, D. L. Bryce, *Chem. A Eur. J.* **2013**, *19*, 11949-11962. c) R. E. Taylor, P. A. Beckmann, S. Bai, C. Dybowski, *J. Phys. Chem. C* **2014**, *118*, 9143-9153. d) R. J. Attrell, C. M. Widdifield, I. Korobkov, D. L. Bryce, *Cryst. Growth Des*. **2012**, *12*, 1641-1653.
[40] a) H. Hamaed, E. Ye, K. Udachin, R. W. Schurko, *J. Phys. Chem. B* **2010**, *114*, 6014-6022. b) L. A. O'Dell, I. L. Moudrakovski, *Chem. Phys. Lett*. **2013**, *565*, 56-60.
[41] H. Hamaed, M. W. Laschuk, V. V. Terskikh, R. W. Schurko, *J. Am. Chem. Soc*. **2009**, *131*, 8271-8279.
[42] K. J. Harris, A. Lupulescu, B. E. G. Lucier, L. Frydman, R. W. Schurko, *J. Magn. Reson.* **2012**, *224*, 38-47.
[43] B. E. G. Lucier, K. E. Johnston, W. Xu, J. C. Hanson, S. D. Senanayake, S. Yao, M. W. Bourassa, M. Srebro, J. Autschbach, R. W. Schurko, *J. Am. Chem. Soc*. **2014**, *136*, 1333-1351.
[44] P. Mastrorilli, S. Todisco, A. Bagno, V. Gallo, M. Latronico, C. Fortuno, D. Gudat, *Inorg. Chem*. **2015**, *54*, 5855-5863.
[45] K. J. Harris, S. L. Veinberg, C. R. Mireault, A. Lupulescu, L. Frydman, R. W. Schurko, *Chem. A Eur. J.* **2013**, 19, 16469-16475.
[46] S. Wi, Z. Gan, R. Schurko, L. Frydman, *J. Chem. Phys*. **2015**, *142*, 064201.
[47] M. Pasero, A. R. Kampf, C. Ferraris, I. V. Pekov, J. R. Rakovan, T. J. White, *Eur. J. Mineral*. **2010**, *22*, 163-179.
[48] a) D. G. Cory, *Chem. Phys. Lett*. **1988**, *152*, 431-434. b) P. Reinheimer, J. Hirschinger, P. Gilard, N. Goetz, *Magn. Reson. Chem*. **1997**, *35*, 757-764.
[49] C. Lejeune, C. Coelho, L. Bonhomme-Coury, T. Azaïs, J. Maquet, C. Bonhomme, *J. Magn. Reson*. **2005**, *27*, 242-246.
[50] F. Audubert, J. Carpena, J. L. Lacout, F. Tetard, *Solid State Ionics* **1997**, *95*, 113-I19.
[51] F. Audubert, PhD thesis, Mise au point d'une matrice apatitique pour le confinement de l'iode-129, Institut National Polytechnique de Toulouse, 1995, n° 1072.
[52] C. Eychenne-Baron, F. Ribot, C. Sanchez, *J. Organomet. Chem.* **1998**, *567*, 137-142.
[53] L. Van Lokeren, R. Willem, D. van der Beek, P. Davidson, G.A. Morris, F. Ribot, *J. Phys. Chem. C* **2010**, *114*, 16087-16091.
[54] F. Ribot, D. Minoux, C. Sanchez, *Mater. Res. Soc. Symp. Proc.* **2001**, *628*, CC2.2.1-CC2.2.6.
[55] G. Metz, X. L. Wu, S. O. Smith, *J. Magn. Reson. A* **1994**, *110*, 219-227.
[56] P. Giannozzi *et al.*, *J. Phys.: Condens. Matter* **2009**, *21*, 395502.
[57] J. P. Perdew, K. Burke, M. Ernzerhof, *Phys. Rev. Lett*. **1996**, *77*, 3865-68.
[58] N. Troullier, J. L. Martins, *Phys. Rev. B* **1991**, *43*, 1993-2006.
[59] L. Kleinman, D. Bylander, Phys. Rev. Lett. **1982**, 48, 1425-1428.
[60] http://theossrv1.epfl.ch/Main/Pseudopotentials
[61] C. Pickard, F. Mauri, *Phys. Rev. B* **2001**, *63*, 245101.
[62] P. Pyykkô, *Mol. Phys.* **2008**, *106*, 1065.
[63] D. Massiot, F. Fayon, M. Capron, I. King, S. Le Calvé, B. Alonso, J.-O. Durand, B. Bujoli, Z. Gan, G. Hoatson, *Magn. Res. Chem*. **2002**, *20*, 70-76.
[64] G. Renaudin, P. Laquerrière, Y. Filinchuk, E. Jallot and J.-M. Nedelec, *Journal of Materials Chemistry*, **2008**, *18*, 3593-3600.
[65] M.C. Stennett, I.J. Pinnock, N.C. Hyatt *Journal of Nuclear Materials* **2011**, *414*, 352–359
[66] F. Audubert, J.-M. Savariault, J.-L. Lacout *Acta Cryst*. **1999**, *C55*, 271-273
[67] J. Tegenfeldt, U. Haeberlen, *J. Magn. Reson.* **1979**, *36*, 453-457.
[68] C. Coelho, T. Azais, L. Bonhomme-Coury, G. Laurent, C. Bonhomme, *Inorg. Chem.* **2007**, *46*, 1379-1387.
[69] J.-B. d'Espinose de Lacaillerie, C. Fretigny, D. Massiot, *J. Magn. Reson*. **2008**, *192*, 244-251.
[70] F. Vasconcelos, S. Cristol, J.-F. Paul, L. Delevoye, F. Mauri, T. Charpentier, G. Le Caër, *J. Phys.: Condens*. *Matter* **2013**, *25*, 255402.

[71] *Multidimensional Solid-State NMR and Polymers*, K. Schmidt-Rohr, H. W. Spiess, Academic Press, 1994.
[72] S. G. Jantz, L. van Wüllen, A. Fisher, E. Libowitzki, E. J. Baran, M. Weil, H. A. Höppe, *Eur. J. Inorg. Chem.* **2016**, *7*, 1121-1128.